Coherent control of terahertz emission and carrier populations in semiconductor heterostructures

I. Brener,* P. C. M. Planken,† and M. C. Nuss

AT&T Bell Laboratories, 101 Crawfords Corner Road, Holmdel, New Jersey 07733-3030

Marie S. C. Luo and Shun Lien Chuang

Department of Electrical and Computer Engineering, University of Illinois at Urbana–Champaign, Urbana, Illinois 61801-2991

L. Pfeiffer

AT&T Bell Laboratories, 600 Mountain Avenue, Murray Hill, New Jersey 07974

D. E. Leaird

Bellcore, Red Bank, New Jersey 07701

A. M. Weiner

School of Electrical Engineering, Purdue University, West Lafayette, Indiana 47907–1285

Received February 14, 1994, revised manuscript received April 15, 1994

A short laser pulse exciting semiconductor heterostructures will induce a time-varying polarization that in turn leads to the generation of terahertz radiation. Although there are several possible mechanisms for this time-dependent polarization, some depend critically on the dephasing time of the photoexcited carriers. For long dephasing times it is possible to control both the populations and the coherence of these particles by proper shaping of the optical pulse. We discuss our recent experimental and theoretical work on coherent terahertz radiation emitted from semiconductor heterostructures when the exciting optical fields are shaped in both amplitude and phase. Our shaping techniques include phase-locked pulse generation in a Michelson interferometer and pulse-train generation by phase-only filtering.

1. INTRODUCTION

Coherent optical excitation of simple multilevel systems with dipole-allowed transitions has drawn considerable attention for many years. By studying these systems in gases, liquids, or solids with optical fields we can gain insight into fundamental issues of quantum mechanics. Thus a variety of experimental techniques have been devised in what is usually called the study of coherent phenomena. The **phase** of the quantum-mechanical system is therefore an important quantity, and its initial state is determined by the exciting optical field. This phase can be lost by a variety of processes, mostly by scattering, and the dephasing time is characteristic of the system and its environment. Isolated molecules or atoms can have very long dephasing times to as long as several seconds, whereas dephasing times of excitonic transitions in semiconductors can be as short as a few hundred femtoseconds.

To study the time evolution of such a system after its initial excitation by an optical field, we would like to monitor the exact quantum state of each level in our system and at every instant. This information is usually inaccessible, and thus we must resort to indirect measurements. A very powerful group of measurements in this respect is optical studies of coherent processes. Coherent phenomena in semiconductor heterostructures have been studied by a variety of optical techniques, such as four-wave mixing, stimulated Raman scattering, and photon echoes. Most of these techniques rely on third-order susceptibilities $\chi^{(3)}$, and usually all the phase information is lost, as the measured quantity is typically the intensity of an optical field. Recent interferometric measurements of resonant four-wave mixing signals overcome some of the limitations of conventional four-wave mixing measurements,[1,2] but to our knowledge these measurements have not been combined with multiple-pulse excitation. Recently several groups measured electromagnetic radiation from a whole family of coherent $\chi^{(2)}$ processes in multilevel systems in semiconductor heterostructures.[3–6] The electromagnetic radiation lies in the terahertz (THz) range, and both the amplitude and the phase can be measured through coherent THz detection. Figure 1 shows a schematic drawing of an n-level system that is excited by an optical field that can be arbitrarily shaped in time, in both amplitude and phase. Before the phase of the excited transitions is lost, different coherent processes can lead to electromagnetic radiation frequencies corresponding to transitions within the n-level system. Such multilevel systems can be implemented in semiconductor

0740-3224/94/122457-13$06.00

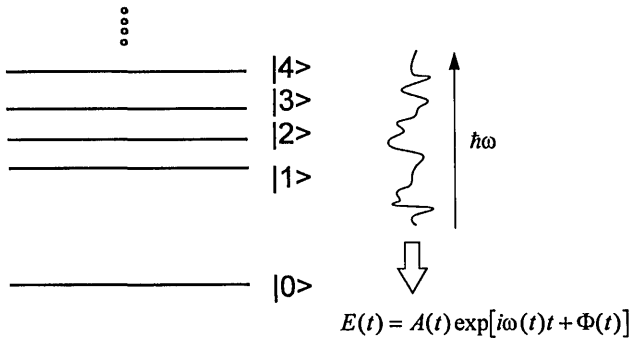

Fig. 1. Schematic diagram of a multilevel system that is excited by an optical field shaped in both amplitude and phase as a function of time. Active manipulation of the quantum interferences between the different levels in the system is possible by proper shaping of the optical field. Also, before the phase of the excited transitions is lost, different coherent processes can lead to electromagnetic radiation at frequencies corresponding to transitions within the n-level system.

heterostructures, and more details will be given in the sections below.

In this paper we review our recent experimental and theoretical research on coherent THz radiation emitted from semiconductor heterostructures when the time evolution of the exciting optical fields is shaped in both amplitude and phase. We also expand our previous work with additional measurements and discussions. We used two main techniques for shaping the exciting optical field: (i) pulse-train generation through phase-only filtering and (ii) Michelson interferometry for generation of a phase-locked pulse pair. The combination of optical excitation with control over the optical phases with the ability to detect both the amplitude and the phase of the emitted THz fields is a unique and invaluable tool in the study of coherent phenomena. Although the experiments described in this paper have been conducted in excitonic levels in semiconductors, this technique can readily be adapted to other physical systems not necessarily in the solid-state phase.

Several experiments have been performed in the past that used pulses with a fixed phase difference, such as the measurement of the optical-coherence decay in sodium gas[7] and iodine[8] and the observation of Ramsey interference fringes in two-photon spectroscopy[9] and of interference between vibrational wave packets in iodine.[10] In all these experiments the measured quantity was the visible fluorescence between two levels. A variety of multiple-pulse experiments have been conducted in the past, as there are several advantages over single-pulse excitation. For example, multiple-pulse experiments provide enhanced frequency selectivity compared with single-pulse excitation and thus can be used to study processes that have closely spaced frequencies, such as molecular systems.[11] Pulse sequences with control over their optical phases can be used to distinguish between coherent and incoherent processes, as in the case of multiphoton ionization.[12] Repetitive excitation was also used to study impulsive stimulated Raman scattering,[13] where it was shown that a particular vibrational mode could be selectively enhanced by matching of the sequence-repetition rate to the vibrational frequency.

This paper is organized as follows. Section 2 contains the appropriate theoretical background on which the rest of the paper is based; in Section 3 we present a description of the experimental techniques and the samples used in this study. Our work in coherent control of THz emission by use of a pair of phase-locked pulses is described in Section 4. In Section 5 we show the results that we obtain when the exciting optical field is shaped as variable-repetition pulse trains. Section 6 describes our research on THz emission from coherent population changes in quantum wells. Finally, a summary and conclusions are presented in Section 7.

2. THEORY AND BACKGROUND: TERAHERTZ EMISSION FROM COHERENT PROCESSES IN QUANTUM WELLS

A short laser pulse exciting a semiconductor sample will give rise to THz emission from the sample into free space. The source of this radiation can readily be understood from Maxwell's equations, as any time-varying polarization will be followed by the radiation of an electric field: $E_{\mathrm{THz}} \propto \partial^2 P(t)/\partial t^2$. There are several possible sources for the generation of such a time-dependent polarization. The most common one is the acceleration of the photogenerated electrons by the surface depletion field. The other source follows from either the creation or the annihilation of polarized electron–hole pairs or from particular cases of a time-varying coherence. The last-named process can be understood when we consider a three-level system such as that depicted in Fig. 2 and solve the optical Bloch equations (the extension to more levels is obvious):

$$\frac{\mathrm{d}\rho}{\mathrm{d}t} = \frac{i}{\hbar}[\rho, H] + \frac{\rho}{T}, \tag{1}$$

where ρ is the density matrix (3×3 in our three-level system), H is the interaction Hamiltonian, and T is a matrix describing the relaxation times between the different levels. Thus T_{11} is the lifetime of level 1, T_{12} is the dephasing time between levels 1 and 2, and so forth.

The time-dependent polarization in this system is given by[14]

$$P(t) \propto |e|\{(z_{33} - z_{11})\rho_{11}(t) + (z_{33} - z_{22})\rho_{22}(t) - 2z_{12}\,\mathrm{Re}[\rho_{12}(t)]\}, \tag{2}$$

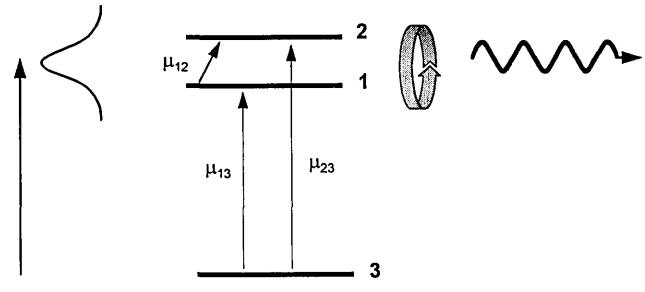

Fig. 2. Schematic drawing of a three-level system with allowed dipole transitions between all three levels. Quantum beats between levels $|1\rangle$ and $|2\rangle$ after coherent excitation by a short laser pulse lead to electromagnetic radiation. In our case this radiation is in the THz range.

where $(z_{ii} - z_{jj})$ is the permanent dipole moment between levels i and j and the far-infrared radiation is given by

$$E_{\mathrm{THz}} \propto \frac{\partial^2}{\partial t^2} P(t). \tag{3}$$

We can now identify two contributions to the THz emission. First, the ρ_{11} and the ρ_{22} terms correspond to changes in the populations of the excited states of the three-level system. They describe the THz emission from quantum-well samples when **polarized** electron–hole pairs are created by photons with energy lower than the barrier energy.[4] The second contribution to this emission is caused by a time-varying coherence ρ_{12} combined with the existence of a dipole moment between levels $|1\rangle$ and $|2\rangle$. The latter contribution occurs, for example, in some semiconductor quantum-well samples in which two excitonic levels can be excited simultaneously by a short laser pulse. Provided that the dipole transition between levels $|1\rangle$ and $|2\rangle$ is allowed, quantum-mechanical arguments dictate that we should observe quantum beats between these two levels followed by an oscillating dipole moment. These quantum beats are usually called charge oscillations and lead to the emission of electromagnetic radiation at a frequency corresponding to the quantum-beat period. Thus quantum beats and radiating charge oscillations are not synonyms: the latter require the existence of the dipole transition moment z_{12} and will lead to emission of THz radiation from the sample only when this requirement is met.[3,5]

An analytical solution to the optical Bloch equation is usually not possible. However, we can obtain a solution if we make a number of assumptions: (i) the laser pulses are delta functions in time and (ii) we perform a second-order expansion in the optical field under the rotating-wave approximation. For example, for a pair of phase-locked laser pulses the laser-excitation function will be $E_L(t) = E_0\delta(t) + E_0 \exp(i\Phi)\delta(t - \tau)$. Φ is the relative optical phase between both pulses, and τ is the delay between them. If, for the sake of clarity, we assume infinite relaxation-time constants, then the coherence $\rho_{12}(t)$ will be

$$\begin{aligned}\rho_{12}^{(2)}(t) = \frac{\mu_{13}\mu_{32}}{\hbar^2} E_0{}^2\{&\exp(-i\omega_{12}t)\theta(t) \\ &+ \exp[-\omega_{12}(t - \tau)]\theta(t - \tau) \\ &+ \exp(-i\Phi)\exp[-i\omega_{12}(t - \tau)] \\ &\times \exp(-i\Delta_{13}\tau)\theta(t - \tau) + \exp(i\Phi) \\ &\times \exp[-i\omega_{12}(t - \tau)]\exp(i\Delta_{23}\tau)\theta(t - \tau)\}.\end{aligned} \tag{4}$$

In Eq. (4), $\omega_{12} = \omega_{13} - \omega_{23}$, $\theta(t)$ and $\theta(t - \tau)$ are Heaviside step functions, and $\Delta_{13} = \omega_{13} - \Omega_L$ and $\Delta_{23} = \omega_{23} - \Omega_L$ are the frequency detunings of the laser with respect to the $3 \rightarrow 1$ and the $3 \rightarrow 2$ transitions. The dipole moments for the transitions $3 \rightarrow 1$ and $3 \rightarrow 2$ are μ_{13} and μ_{23}, respectively. The extension to multiple-pulse excitation is easy if we make the same assumptions. We can obtain significant physical insight into the processes described in this paper by examining Eq. (4). The response of the system to the double-pulse excitation bears a resemblance to Young's optical double-slit experiment. The first two terms in Eq. (4) correspond to the response of the system to two individual pulses. The last two terms describe interference between the polarizations (and the wave functions) set by each pulse in the pair. This interference depends on the detunings Δ_{13} and Δ_{12} and the optical phase difference Φ.

The calculation of the THz radiation caused by the diagonal terms of the density matrix ρ in Eq. (1) is not so simple. In these cases we solve the linearized Bloch equation numerically, using a fourth-order Runge–Kutta method. The generation of THz radiation by the **creation** of a polarized state (e.g., a polarized e–h pair) does not require a long coherence time. Thus, when we excite our system with a single short laser pulse, the THz radiation will adiabatically follow the integral of the exciting pulse. This radiation will be quite near a single cycle of the electromagnetic field when the exciting pulses are subpicosecond. However, if more than one pulse is used for excitation and if the dephasing time is longer than the pulse separation, then the interference between the wave functions created by the different pulses can also lead to changes in **populations**. Hence coherent processes will also be important in this THz-radiation-generation scheme.

3. EXPERIMENT

In this study we use two $GaAs/Al_xGa_{1-x}As$ as samples in which the existence of excitonic charge oscillations was successfully demonstrated in previous research[3,5]: (a) a double-coupled quantum well (DCQW) consisting of 10 repetitions of a 10-nm narrow well and a 14.5-nm-wide well separated by a 2.5-nm $Al_{0.2}Ga_{0.8}As$ barrier and (b) a multiple-quantum-well sample consisting of 15 periods of 17.5-nm GaAs wells separated by 15 nm of $Al_{0.3}Ga_{0.7}As$ barriers. To apply a variable electric field in the direction perpendicular to the layers, we evaporate semitransparent chromium contacts on top of the samples. An electric field can then be applied between the Schottky contact and the n-doped substrate. Schematic representations of the energy levels in the two samples are presented in Fig. 3. These samples were used to demonstrate THz emission from charge oscillations caused by quantum beats between two excitonic levels.[3,5] The exciton levels in both samples behave as quasi-three-level systems. In sample (a) the two excited upper states $|1\rangle$ and $|2\rangle$ are the bonding and the antibonding exciton levels of the narrow well; in sample (b) these are the heavy- and the light-hole exciton levels. In

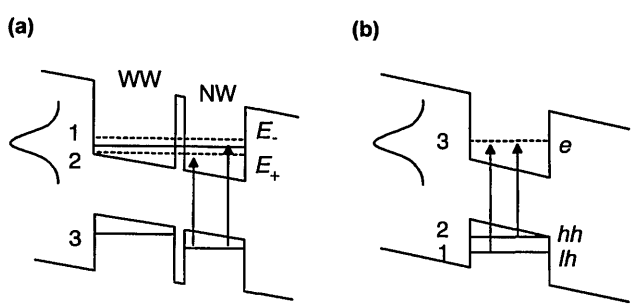

Fig. 3. Schematic energy-level diagram for (a) the DCQW and (b) the single-quantum-well (SQW) samples. The excitonic levels depicted in the diagram can be regarded as a quasi-three-level system.

these samples dipole transitions are permitted between all three levels (even with no applied electric field). This effect is in contrast to atomic and molecular systems, in which optical selection rules make a dipole transition between the upper two states forbidden as long as the system has inversion symmetry. This inversion symmetry is broken in our samples because of the asymmetric double well in sample (a) and because of valence-band mixing in sample (b).[5,15] When levels $|1\rangle$ and $|2\rangle$ are excited coherently with a broadband short laser pulse, charge oscillations that are due to quantum beats between these two levels occur with a beat frequency of $\Delta E/h$, where $\Delta E = E_1 - E_2$. These charge oscillations produce a time-dependent polarization $P(t)$ that radiates. The application of an electric field allows for continuous tuning of the energy positions of the excitonic levels and has a different effect, depending on the sample being used. In the coupled-quantum-well sample we typically apply an electric field such that the $n = 1$ excitonic levels are energetically aligned.[3] In the other sample we work around flat-band conditions.

The optical pulses used in our experiments are generated by an argon-ion-pumped Ti:sapphire laser that produces ~80-fs pulses tunable near 800 nm. The beam is then split into two: a weak part is used to gate the photoconductive antenna, and the more intense beam undergoes pulse shaping and is used to excite the sample mounted in a cryostat. We then use two different setups for the generation of either a single phase-locked pulse pair or variable-repetition-rate pulse trains (discussed in the remainder of this section). The pulse sequence is then focused on the sample, with a typical spot size of 1–2 mm and a pulse energy of roughly 1 nJ. The generated THz radiation is collected, collimated with a pair of off-axis parabolic mirrors, and focused onto a 50-μm photoconducting dipole antenna[16] equipped with a hyperhemispherical silicon substrate lens, as is shown in Fig. 4. We measure the electric field $E(t)$ emitted from the sample by recording the photocurrent from the antenna as a function of the delay between the gating pulse and the exciting shaped pulse (either a pair or a train). With the typical excitation power and spot size that we use, the carrier densities are roughly 10^{10} cm^{-2}. The bandwidth of the short laser pulses is wide enough so that it spectrally overlaps the two excitonic transitions that we want to excite simultaneously. In some experiments we also artificially reduce the bandwidth of the exciting optical field. This is important when we want to avoid the generation of free electron–hole (e–h) pairs.

The first of the pulse-shaping setups is used to generate a pair of phase-locked pulses and consists of a Michelson interferometer, as shown in Fig. 4. One of the arms of the interferometer is mounted upon a delay stage so that the pulses emerging from the interferometer can be delayed in time. One of the end mirrors of the Michelson interferometer is mounted upon a piezoelectric transducer (PZT) for active stabilization of the length of the arm to within a fraction of a wavelength. After being dispersed by a grating, the output of the interferometer illuminates a pair of photodiodes, providing feedback to the PZT. This scheme locks the spectrum of the pulse pair on a spatially separated photodiode pair. We can control the coarse delay between the two pulses emerging from the Michelson interferometer by varying the delay on the delay stage. The optical phase difference between the two pulses is then set by movement of the photodiode pair, which fine-tunes the PZT. The latter can be controlled with great accuracy, and we can routinely adjust this phase difference to any value between 0 and π (delay of less than 1.3 fs).

The second setup is a pulse shaper that can transform a single femtosecond pulse into a train of equally spaced pulses by use of phase-only filtering.[17] It consists of two gratings and two lenses arranged as a unity magnification system, as is shown in Fig. 5. A fused-silica phase mask that contains phase patterns fabricated by microlithography and reactive-ion etching is placed in the Fourier plane of the pulse shaper to modify the electric-field spectrum so as to produce the desired pulse train.[18] The information contained in the phase mask is binary, and each pixel corresponds to a phase delay of 0 or π. One accomplishes this effect by etching certain pixels to a depth of $\sim\lambda$. The spatial frequency of the phase mask determines the frequency of the pulse train, which can be tuned from 1.4 to 2.6 THz by translation of different phase patterns with different spatial frequencies into the beam. A schematic description of the phase mask is shown in Fig. 5; the arrow represents the movement axis used to bring different phase patterns into the focused and dispersed beam. This operation allows for the tuning of the repetition rate in steps of ~130 fs. Examples of generated pulse trains of 1.4 and 2.5 THz are shown in Fig. 6.

4. COHERENT CONTROL OF TERAHERTZ EMISSION WITH TWO PHASE-LOCKED PULSES

As we discussed in Section 2, the THz radiation caused by charge oscillations in our quasi-three-level systems will be directly influenced by the optical phase difference between the two pulses when we excite our samples with a phase-locked pulse pair. This THz radiation in turn reflects the amplitude and the phase of the excitonic wave functions excited by the optical field. In this section we show how we can enhance, weaken, and induce large phase shifts in the excitonic charge oscillations observed in our heterostructure samples.[19] Our experiments provide a unique opportunity, as we can obtain information on the **phase** of the **excitonic wave functions.** This is pos-

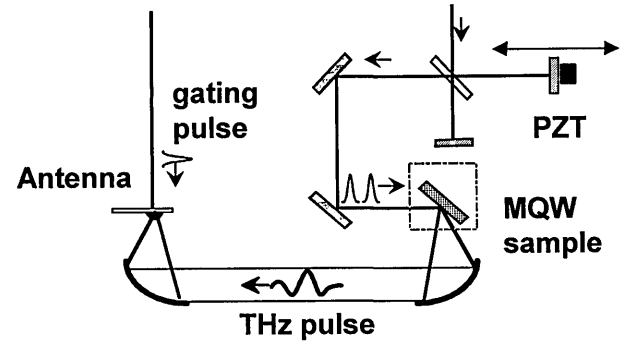

Fig. 4. Experimental setup consisting of a Michelson interferometer for the generation of a phase-locked pulse pair and the THz-detection part. MQW, multiple quantum well; PZT, piezoelectric transducer.

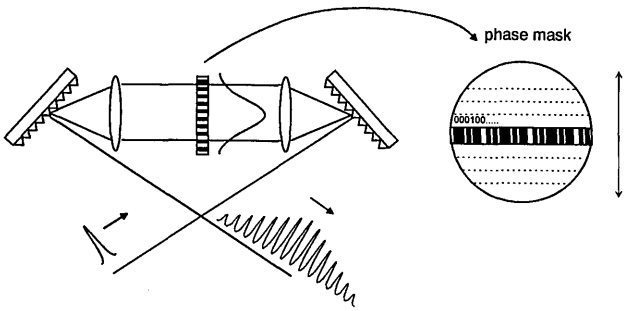

Fig. 5. Schematic diagram of the pulse shaper used to generate the pulse trains and of the phase mask that is placed in the Fourier plane of the shaper. The dotted lines represent the same phase patterns but with different spatial frequencies. The arrow shows the direction of translation of the mask when the repetition rate of the train is changed.

sible only because we can time resolve both the amplitude and the phase of the electromagnetic radiation emitted by the charge oscillations.

We present two sets of measurements according to the time delay between the pulses of the pulse pair. Let us first consider the case in which both pulses are separated by an integer number of the quantum-beat period, namely, $\tau = 2T_{12} \equiv 2|2\pi/\omega_{12}|$ [with $\omega_{12} = (E_1 - E_2)/\hbar$]. The detected THz waveforms for several values of the phase difference Φ are shown in Fig. 7. Traces (a) and (b) show the THz radiation caused when only one of the pulses (either the first or the second one) excites the sample. Traces (c) and (d) are the THz waveforms that result when both pulses are present in the sample. Trace (c) corresponds to $\Phi = 0$, and we clearly see a threefold enhancement of the THz radiation. When $\Phi = \pi$ [trace (d)] the arrival of the second pulse almost eliminates the THz radiation. This result demonstrates our ability to turn the THz radiation on or off by an adjustment of merely 1.3 fs in the pulse delay. These results can readily be understood if we look at the power spectrum of the pulse pair. The intensity I of the superposition of two coherent electric fields E_A and E_B is

$$I = |E|^2 = |E_A + E_B \exp(i\Phi)|^2$$
$$= |E_A|^2 + |E_B|^2 + 2E_A E_B \cos(\Phi). \quad (5)$$

If $E_A = E_B$, then constructive interference ($\Phi = 0$) increases the intensity of the field by a factor of 4 (which will in turn increase the intensity of the emitted THz radiation by a factor of 4). However, destructive interference ($\Phi = \pi$) cancels the exciting field, and therefore no excitons are excited in the system.

These arguments fail when the pulse separation is not an integer multiple of the quantum-beat period. The experimental measurements for the case of $\tau = 2.5T_{12}$ are shown in Fig. 8. Traces (a) and (b) show the THz waveforms that result when only one of the laser pulses excites the sample. Trace (c) shows the measured THz field that results when both pulses excite the sample with $\Phi = 0$. In this case we measure only a slight increase in amplitude but a large **phase shift** in the THz radiation of $-\pi/2$ [we can see this effect by following the dashed vertical line and the arrow on trace (c)]. An opposite phase shift of $\pi/2$ in the emitted THz radiation is measured when the $\Phi = \pi$ [trace (d)]. Another interesting case is shown in trace (e) for $\Phi = \pi/2$, where the THz signal is weakened but not canceled. The power arguments do not work in this case, and a more satisfactory way to understand these effects is through the use of a pseudovector representation.[15,20] We can represent the four terms of Eq. (4) by pseudovectors rotating at the quantum-beat frequency ω_{12}. In the discussion immediately below we assume that $\Delta_{23}T = -\Delta_{23}T = \pi/2$, which means that we pump in the middle of levels 2 and 3. When the delay between the pulses in the pulse pair corresponds to an integer number of the quantum-beat period, terms 1 and 2 of Eq. (4) are collinear. The phase Φ determines what happens to terms 3 and 4: for $\Phi = 0$ we obtain a complete alignment of all the terms [constructive interference; see Fig. 9(a)], whereas for $\Phi = \pi$ terms 3 and 4 align antiparallel to terms 1 and 2, leading to destructive interference [Fig. 9(b)]. When the optical pulse separation is a half-integer multiple of T_{12} the first two vectors are antiparallel. For $\Phi = 0(\pi)$, vectors 3 and 4 are parallel but are rotated by 90° (−90°). This result is depicted in Figs. 9(c) and 9(d).

To compare our calculations with the experimental data, we must go beyond the simple qualitative arguments presented in the previous paragraph and include finite pulse duration, dephasing times, and lifetime parameters. We then solve the optical Bloch equations numerically as described in Section 2 with the following parameters: lifetimes $T_{11} = T_{22} = T_{33} = 500$ ps and dephasing times $T_{12} = T_{13} = T_{23} = 2.75$ ps.[21] In Figs. 10 and 11 we plot $\mathrm{Re}[\rho_{12}(t)]$, as the THz electric field is proportional to this quantity. In principle, a comparison between theory and experiment should include convolution of the theoretical curve with the photoconductive-antenna response. Because we lack the latter information, we plot the real part of the coherence term directly. Even without this convolution the agreement between theory and experiment is extremely good. Figure 10 shows the results of our calculations for the same experimental conditions as are shown in Fig. 7, i.e., for $\tau = 2T_{12}$ and $\Phi = 0, \pi$. The theoretical calculations for

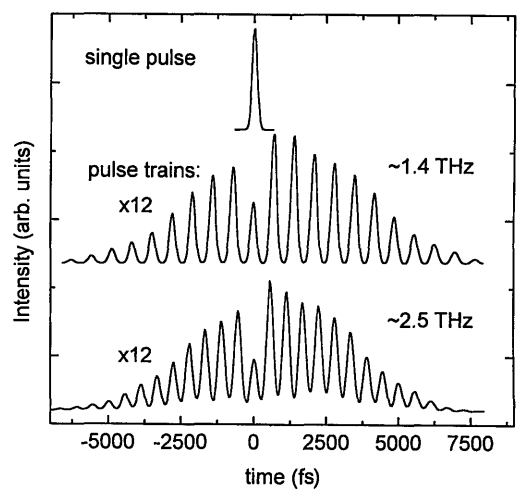

Fig. 6. Cross-correlation measurements of two pulse trains generated with the setup shown in Fig. 5. The upper trace is a cross correlation measured when the phase mask is removed from the Fourier plane of the pulse shaper.

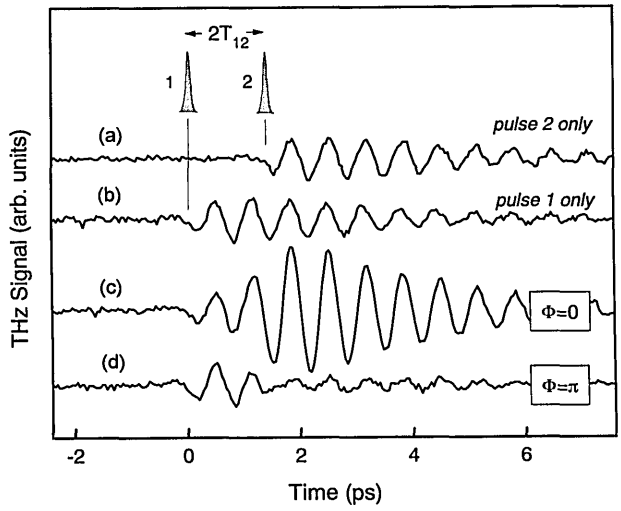

Fig. 7. (a), (b) Measured THz waveforms when single pulses excite the sample. (c), (d) Waveforms measured when both pulses excite the sample with a delay of $2T_{12}$ and two values of the phase difference Φ.

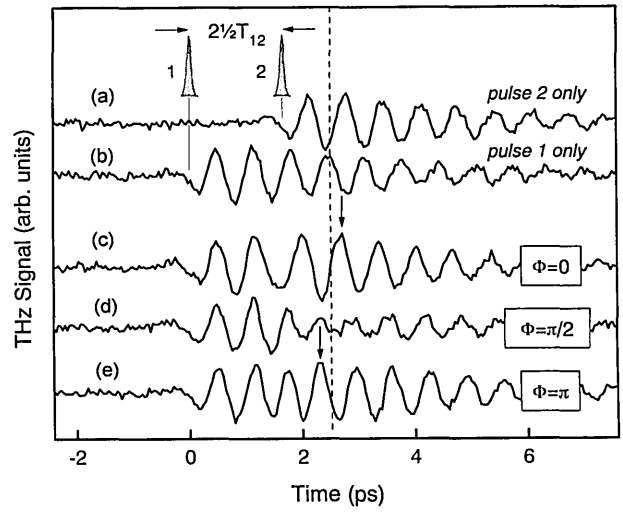

Fig. 8. (a), (b) Measured THz waveforms when single pulses excite the sample. (c)–(e) Waveforms measured when both pulses excite the sample with a delay of $2.5T_{12}$ and three values of the phase difference Φ. The vertical solid and dashed lines permit visualization of the phase shift of the emitted THz radiation at the arrival of the second pulse.

the case depicted in Fig. 8 are shown in Fig. 11, and we can reproduce all the main features of this case, namely, the different phase shifts and the rise and the decay of the signals, very well.

Thus far we have presented only a microscopic description of the generation of THz radiation from a three-level system. However, there is always a relationship between the microscopic description and the macroscopic susceptibilities.[22] All the processes described thus far can be related to resonant frequency mixing through the second-order nonlinear susceptibility $\chi^{(2)}$ of our three-level system. In all these experiments two visible photons are frequency mixed to generate a single THz photon. There are four different possibilities for the difference-frequency mixing process, as there are four different combinations for both visible photons: they can both come from the first pulse or both come from the second pulse, or they can come from different pulses separated in time. In the last-named case the interaction of these two photons separated in time is possible only through the polarization left in the medium by the first pulse, as long as the second pulse arrives within the dephasing time of the induced polarization (T_{12}).

Finally, we discuss an issue that will become important in the sections below, namely, the relationship between the phase of the exciting pulses and the **populations** of the different levels. Thus far we have presented only the influence of this phase on the coherence term ρ_{12} and hence on the THz radiation caused by charge oscillations. However, the effects of destructive and constructive interference also apply to the **real populations** of the excitonic levels. One can visualize these coherent population effects by plotting the population terms ρ_{11} and ρ_{22} for the same experimental conditions as are shown in Fig. 7. This process is shown in Fig. 12 for the ideal case of infinite dephasing times and lifetimes, $\tau = 2T_{12}$, and for excitation at the middle of levels $|1\rangle$ and $|2\rangle$. We can clearly see that when the second pulse excites the sample with $\Phi = 0$ there is also a coherent addition in the population of levels 1 and 2, and therefore ρ_{11} and ρ_{22} experience a fourfold increase at the arrival of the second pulse. When the second pulse has an opposite optical phase, $\Phi = \pi$, the arrival of the second pulse causes **depopulation** of levels $|1\rangle$ and $|2\rangle$. Therefore there is a clear correlation between the coherent effects on the THz radiation and the magnitude of the changes in the populations of the excited states. We use this fact in the sections below for direct manipulation of the populations through adequate shaping of the exciting optical field. These ideas are similar to those used in previous studies in chemistry,[23] where the goal is to control chemical reactions through the active manipulation of quantum interferences.

5. REPETITIVE EXCITATION OF CHARGE OSCILLATIONS

We can extend the ideas presented in Section 4 by considering not one or two short laser pulses with a definite

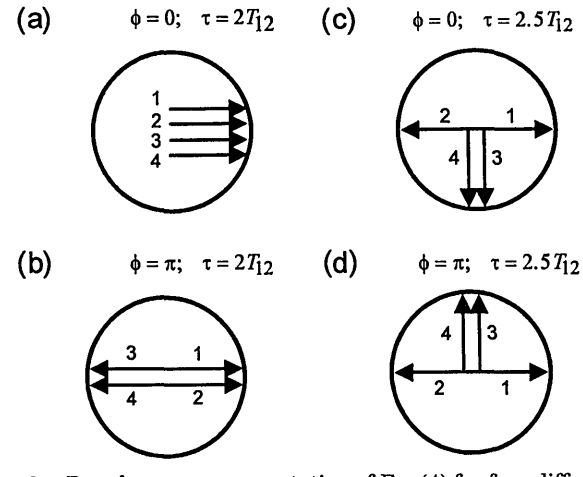

Fig. 9. Pseudovector representation of Eq. (4) for four different combinations of pulse delay and phase difference. In all the cases, pumping is in the middle between levels 1 and 2. Cases (a) and (b) apply to Fig. 7, whereas cases (c) and (d) apply to Fig. 8 and qualitatively explain the observed phase shift.

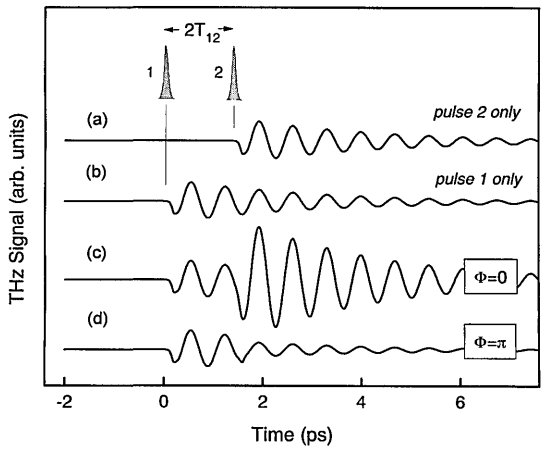

Fig. 10. Theoretical calculation for the case depicted in Fig. 7 [(a)–(d) are same as in Fig. 7], with finite lifetime and pulse width and $T_{12} = 2.75$ ps.

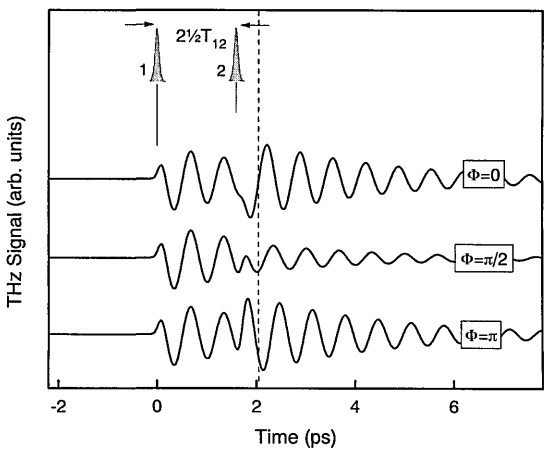

Fig. 11. Theoretical calculation for the experimental results shown in Fig. 8. The parameters used are the same as in Fig. 10 but for a different pulse-pair separation.

optical phase relationship but a pulse train with a variable repetition rate. If we could control the amplitude and the phases of the pulses in the train **independently,** then we could also explore the combined effect of coherent manipulation and repetitive excitation of the charge oscillations. Previous experiments with periodic pulse trains such as impulsive Raman scattering[13] were conducted off resonance, and hence there was no signature of the coherent effects we have shown thus far.

In pulse-shaping techniques there is usually a trade-off between efficiency and phase response: the simplest scheme for the generation of a pulse train out of a single femtosecond pulse is to use an amplitude mask in the Fourier plane of the same pulse shaper shown in Fig. 5. For example, an amplitude mask consisting of a number of equally spaced slits will lead to the generation of a pulse train. In this pulse-train generation each pulse in the train will have the same optical phase. However, this technique is not efficient, and as a consequence of amplitude filtering we lose much of the initial intensity. Phase-only filtering is a much more efficient technique, as amplitudes are not filtered at all. With the proper design (i.e., antireflection coating of the phase mask, etc.) efficiencies near 100% can be achieved. However, the price that one pays is that the optical phases of all the pulses in the train will now be different and will depend on the exact nature of the phase mask and on its position in the Fourier plane. Figure 13 shows the calculated amplitude and optical phase of our generated pulse train for a specific position of the phase mask in the Fourier plane. The phase pattern can be changed by translation of the phase mask one pixel at a time in a direction perpendicular to that shown in Fig. 5.

The lower panel in Fig. 14 shows the THz waveforms obtained when we excite the coupled quantum well at the built-in field (~1.4 kV/cm) with a pulse train that matches the charge-oscillation period.[24] For comparison we show, in trace (a) of Fig. 14, the THz radiation obtained when the phase mask is removed from the Fourier plane (the cross correlation of the exciting pulse is shown in the upper inset). This THz transient clearly shows the charge oscillations with a period of 1.52 THz and a decay time of ~3 ps. We tune the center wavelength of the exciting train to the center of the E_+ and the E_- transitions in the narrow well at $\lambda = 805$ nm. Traces (b) and (c) of Fig. 14 both result when the pulse train excites the sample. The only difference is a horizontal translation of the phase mask in the Fourier plane. In this figure, two features are salient: (i) the THz radiation emitted in case (b) reaches almost the same peak value as in the case of single-pulse excitation, despite the fact that the individual pulses in the pulse train have less than 1/12 the intensity of the single pulse used in case (a), as is

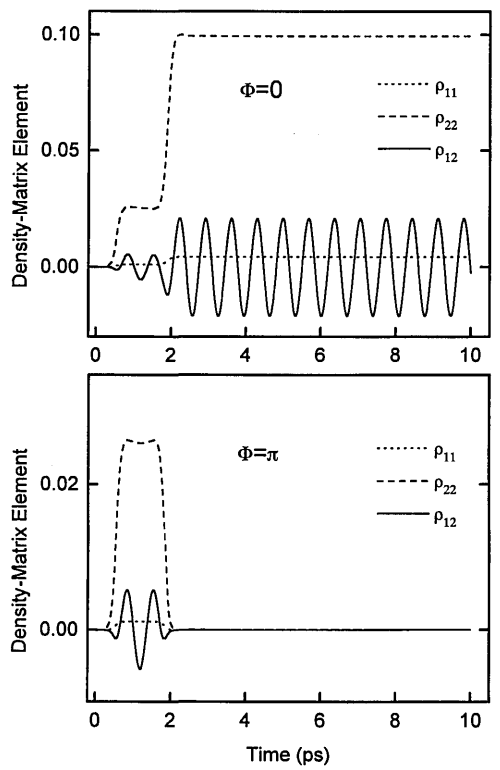

Fig. 12. Time evolution of the populations ρ_{11} and ρ_{22} of the excited states 1 and 2, respectively, and of the coherence ρ_{12} for two cases of phase difference $\Phi = 0$ and $\Phi = \pi$ for a pulse-pair delay of twice the beat period. The parameters used in the calculations match the experimental conditions given in Section 4.

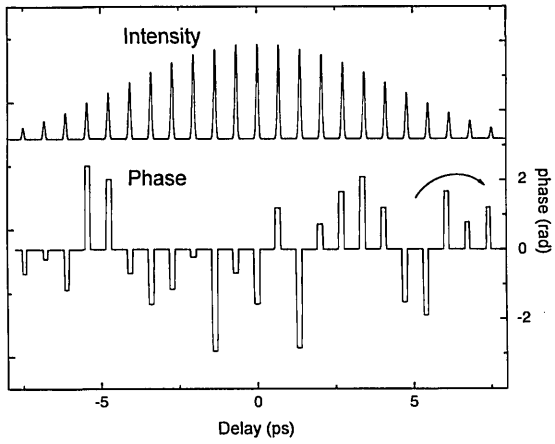

Fig. 13. Calculation of the intensity and phase profiles of the pulse train used in our experiments for a particular position of the phase mask in the Fourier plane.

shown in the upper and the lower insets (this result is a clear indication of forced coherent charge oscillations); (ii) there is almost **no THz radiation for negative delay times** even though the pulse train extends symmetrically to both positive and negative delay times. Feature (ii) is critically dependent on the lateral position of the phase mask, as evidenced by trace (c) of Fig. 14. As trace (b) shows the quantum beats extend to longer delay times compared with those in the case of single-pulse excitation. This result is evident only when the pulse-sequence-repetition rate matches the quantum-beat period. The coherent addition of the THz radiation on excitation with the pulse train and the longer duration of the beats are indicative of sustained charge oscillations. All the main features shown in Fig. 14 are also reproduced in the SQW sample when the laser spectrum overlaps the heavy-hole (hh) and the light-hole (lh) exciton transitions, with the only differences being a shorter dephasing time and a quantum-beat frequency of 1.4 THz. We also investigated the effect of different repetition rates in the exciting pulse train. This is shown in Fig. 15 for the hh–lh sample and for three different repetition rates, one of which is near the resonance frequency of 1.4 THz. As we move further away from the resonance frequency, it is harder to sustain the charge oscillations.

The explanation for the behavior shown in Fig. 14 is closely related to the effects discussed in Section 4, i.e., quantum interferences of the excited-state wave functions. Hence we calculate the THz response of our quasi-three-level system under excitation by the pulse train used in Fig. 14. The amplitude and phase patterns of the pulse train are calculated by Fourier analysis (as was done in Fig. 13), and the solution to the optical Bloch equations is obtained as described in Section 2, with the same parameters as used in Section 3. The fit to trace (b) of Fig. 14 is shown in Fig. 16(a), and we can reproduce the important features remarkably well, such as the canceling of the THz radiation of the first half of the pulse train and the sudden buildup near $\Delta t \sim 0$. As we discussed in Section 4, the cancellations in the coherence ρ_{12} are also accompanied by a cancellation in the exciton **populations**. This can be seen from Fig. 16(b), where we plot the calculated time evolution of the populations of both excited states, ρ_{11} and ρ_{22}. Note the cancellation of the populations for the first half of the pulse train, which is caused by quantum interferences between the **wave functions**. This lack of population buildup despite optical excitation by many pulses is the cause of the absence of THz radiation for almost half the pulse train.

Finally, we discuss measurements performed under the application of an external electric field and with the same excitation scheme, namely, variable-repetition-rate pulse trains. The application of an electric field greatly enhances the instantaneous THz radiation,[4,25] whereas the signal generated by the quantum beats is not lin-

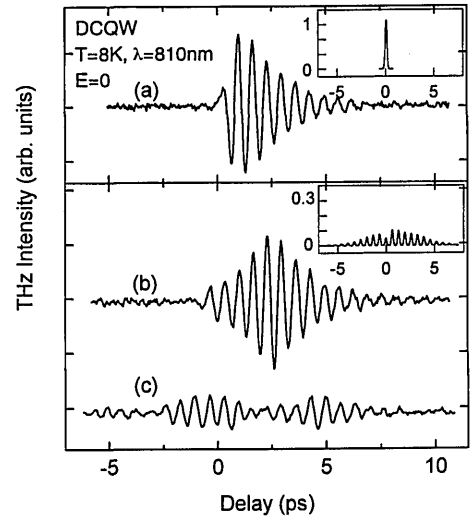

Fig. 14. (a) THz waveform measured after excitation of the DCQW sample by a single short laser pulse overlapping the E_+ and the E_- transitions. The oscillatory signal is due to quantum beats followed by charge oscillations. (b) THz radiation measured after the sample is excited with a pulse train with a repetition rate matching the quantum-beat period of 1.52 THz. (c) Same as (b) but with the phase mask horizontally displaced; this procedure changes the phase pattern of the train but not its intensity. The insets show cross-correlation curves of a single optical pulse with the respective exciting optical fields used.

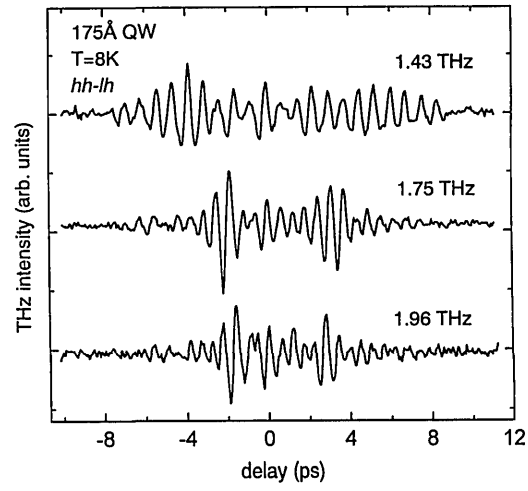

Fig. 15. THz waveforms measured in the DCQW for three different repetition rates of the exciting pulse train. QW, quantum well.

early proportional to the applied field. The enhancement of this instantaneous contribution is due to the field-induced $\chi^{(2)}$ or, in other words, to the breaking of the inversion symmetry caused by the electric field. We would like to know the dephasing time of the e–h pairs that give rise to this instantaneous contribution. Figure 17 shows the same measurements that are presented in Fig. 14 but with the application of an electric field of 11 kV/cm (10 kV/cm) in the DCQW (hh–lh) sample. Also, the excitation wavelength was adjusted to match the Stark-shifted exciton transitions. In both cases the quantum interferences observed before are practically absent, and the THz transients roughly follow the temporal shape of the envelope of the optical-pulse train.[26] Also note that, in contrast to trace (b) of Fig. 14, the THz signal emitted after excitation with the pulse train is much smaller than for the single-pulse case, which indicates a lack of coherent addition and thus an absence of forced oscillations. No significant change in the THz transients is found when the optical phases in the pulse train are varied by horizontal translation of the mask in the Fourier plane. All these results can be understood only if the particles that give rise to the THz emission have a short dephasing time. The application of the electric field does not shorten the exciton dephasing time significantly, as is evidenced by our measurements of the quantum beats for various fields. At large applied electric fields the signal that is due to the creation of polarized e–h pairs dominates the THz radiation emitted from the samples (at flat-band conditions the quantum-beat signal is the dominant one). Therefore the excitation of continuum states becomes more important when a large electric field is applied to the sample. A significant number of free carriers are excited when the bandwidth of the laser pulse is much larger than the exciton linewidth. However, this factor by itself is not enough to explain the short dephasing time evident from the data shown in Fig. 17. We must conclude that at high electric fields the ratio of photogeneration of free carriers versus excitons increases for the same bandwidth of the exciting laser pulse.

6. TERAHERTZ EMISSION FROM COHERENT POPULATION CHANGES

In Sections 4 and 5 we dealt with THz emission that is due to a time-varying polarization caused by processes involving the **coherence** term ρ_{12}, more specifically, quantum beats followed by charge oscillations. As mentioned in Section 2, population changes can also lead to THz emission from semiconductor heterostructures. Previously we showed[4] that the generation of polarized e–h pairs in quantum wells can produce THz radiation. However, no attempt was made to identify the nature of those e–h pairs (excitons or free electron–hole pairs), as in both cases the creation of a polarized state was enough to cause THz emission from the semiconductor sample. This THz emission corresponds to a single cycle of the electrical transient and grows as the integrated pulse energy increases. We can now apply the coherent-control techniques outlined in Sections 4 and 5 for selective modification of the populations of the species with a long dephasing time, namely, the excitons, and to monitor the

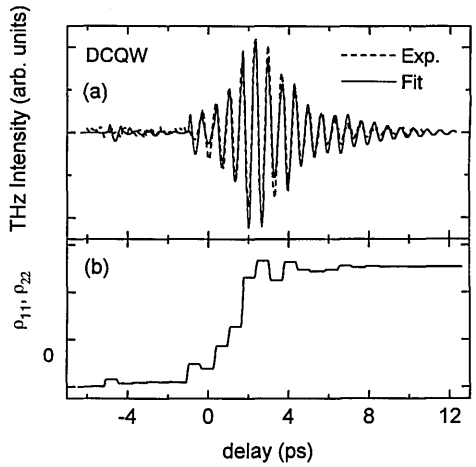

Fig. 16. Experimental THz transient shown in trace (b) of Fig. 14 with the model calculation as described in the text (solid curve). The absence of THz radiation for almost half the pulse train is due to the absence of population buildup of the states $|1\rangle$ and $|2\rangle$. The latter in turn is caused by quantum interferences between these two states. This effect can be seen in (b), where we plot the populations of the excited states.

THz emission from the population changes that occur after photogeneration.[27] Because free e–h pairs have much shorter dephasing times, of the order of 100 fs,[28] they will be insensitive to the process of coherent control. In this case we should measure only THz radiation when these pairs are created but none that is due to any coherent population changes.

The first results we present in this section are measured in sample (b), which shows hh–lh beats when both levels are coherently excited. We chose this sample because there is a clear distinction between the hh exciton and the e–h continuum. The photocurrent spectrum of this sample is shown in Fig. 18. To investigate THz emission from coherent population changes we use

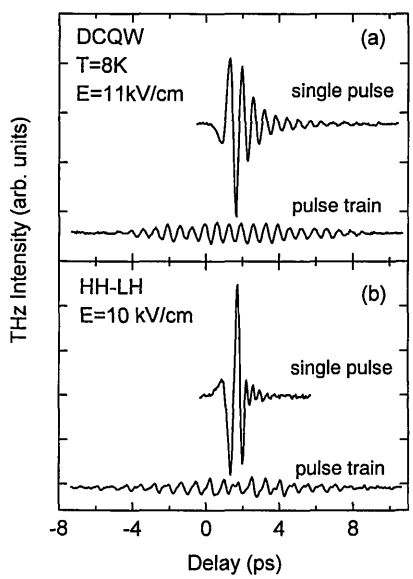

Fig. 17. THz waveforms measured after a single pulse and a pulse train excite (a) the DCQW and (b) the SQW samples and on application of an electric field. Note that unlike for the case shown in Fig. 14 the THz radiation closely follows the intensity of the optical field, and no phase dependence is found.

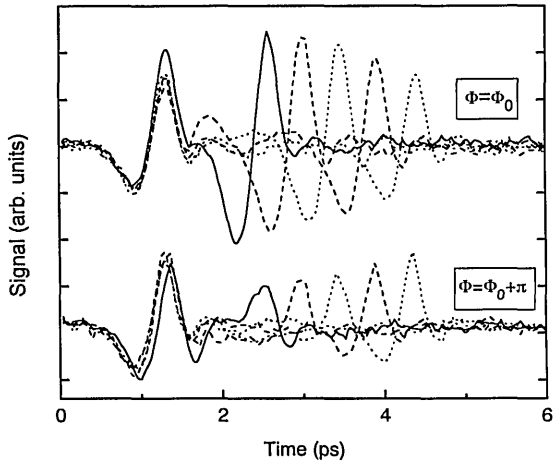

Fig. 19. THz waveforms measured when a pulse pair excites the hh band. The phase difference in the upper (lower) traces was adjusted to maximize (minimize) the THz transient produced at the arrival of the second pulse.

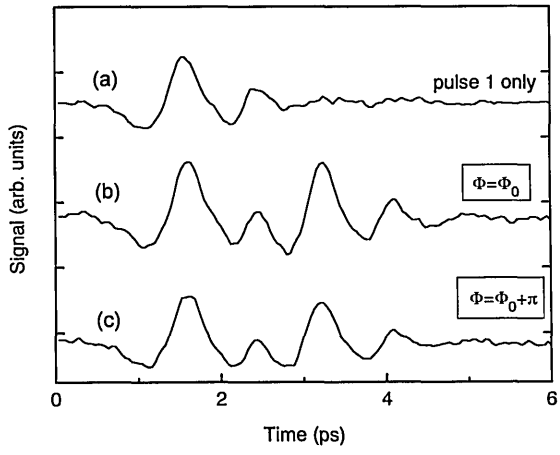

Fig. 20. THz waveforms measured on excitation in the 2D continuum 30 meV above the hh exciton line: (a) THz signal caused by a single pulse; (b), (c) THz signals generated by a phase-locked pulse pair for two different values of the phase difference, respectively.

a phase-locked pulse pair for the optical excitation. Because we want to excite only hh excitons and to avoid the excitation of lh excitons or continuum states, we add a spectral filter to the experimental setup. The effect of this spectral filtering on the high-energy side is shown in Fig. 18. Although this process also lengthens the pulse to a value of ~300 fs, there is still no temporal overlap of the two pulses. Again, the coarse delay is adjusted by means of a delay stage, and the optical phase difference Φ between both pulses is controlled by fine-tuning of the PZT.

We present our results for two typical excitation cases, which are shown in Fig. 18: (i) resonant excitation of hh excitons and (ii) e–h pairs in the two-dimensional (2D) continuum 30 meV above the exciton line. The THz waveforms that are measured when we resonantly excite hh excitons are shown in Fig. 19. We present waveforms measured for five different pulse delays and for two values of the optical phase difference Φ. For the upper traces we adjust the phase to maximize the THz signal generated by the second pulse, and we do the opposite for the lower traces. Clearly, when both pulses are within the dephasing time of the excitons (~3 ps), the optical phase of the second pulse strongly influences the THz transient that it generates. Again, we must remember that the mechanism responsible for this THz-radiation generation includes neither quantum beats nor real transport. All these effects disappear when the second pulse arrives more than 3 ps after the first pulse, in which case the THz waveform resembles the THz transient generated by the first pulse. The next case is shown in Fig. 20, which illustrates what happens when we excite e–h pairs in the 2D continuum. Trace (a) shows the THz waveform that results when a single pulse excites the sample. After recording trace (a), we turn the second pulse on with a time delay of 1.66 ps and with two different values of the optical phase, 0 and π. Apart from changing the excitation energy, the rest of the conditions are similar to those used in Fig. 18. Obviously, the second pulse generates a THz transient almost identical to that generated by the first pulse, and there is no measurable dependence on the optical phase. The difference between the two cases depicted in Fig. 19 and 20 is best illustrated in Fig. 21, in which we plot the peak ampli-

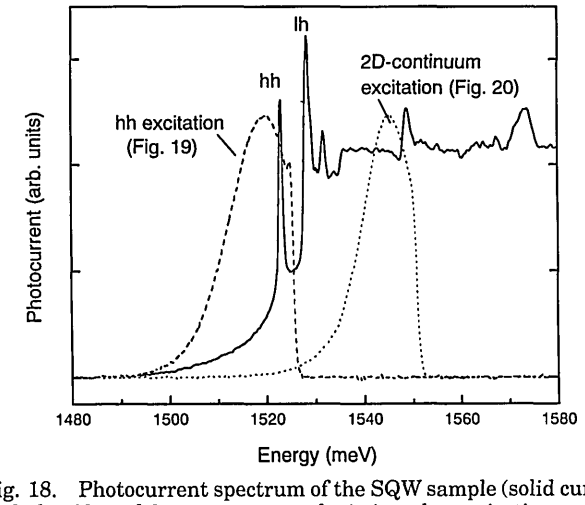

Fig. 18. Photocurrent spectrum of the SQW sample (solid curve) and the filtered laser spectrum depicting the excitation conditions of Figs. 19 and 20 (dashed curves).

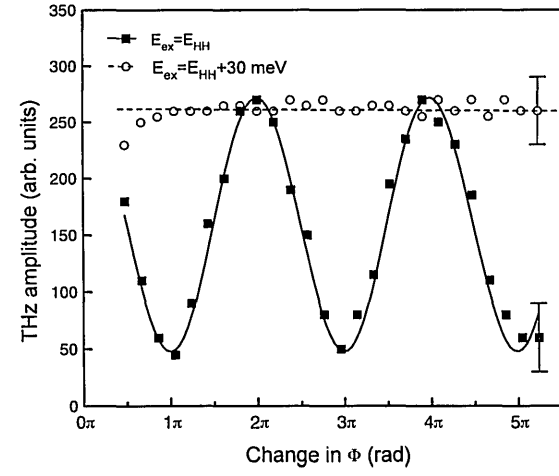

Fig. 21. Peak intensity of the THz transient after excitation with a phase-locked pulse pair versus the phase difference Φ for excitation into the hh band (squares) and into the 2D continuum (circles).

tude of the THz transient generated by the second pulse as a function of the optical phase difference between the two pulses. For this figure we choose a pulse-pair delay of 1.83 ps, which is still less than the exciton dephasing time. A strong modulation in the THz signal can be observed when hh excitons are resonantly excited (squares), but this modulation is absent in the case of excitation into the continuum (circles).

To understand these results we again resort to the arguments used in Sections 2 and 4, namely, the THz radiation from population **changes** that are a combined effect of the coherence left in the medium by the first pulse and the optical phase of the second pulse. When we excite hh excitons we can qualitatively see the effect of the optical phase of the second pulse on the exciton populations by comparison with Fig. 12. Although Fig. 12 shows the calculation for a three-level system, a two-level system shows a similar behavior. For $\tau = T_{12}$ and $\Phi = 0$ the second pulse will increase the population by a factor of 4. For $\Phi = \pi$ the excited state will be depopulated, a process that is essentially stimulated emission (see the discussion below). We can visualize this process by again solving the optical Bloch equations (now for a two-level system) in the ideal case of $E_L(t) = E_0\delta(t) + E_0 \exp(i\Phi)\delta(t - \tau)$. Following the formalism of Section 2, we obtain

$$\rho_{22}^{(2)}(t) = \frac{|\mu_{21}|^2|E_0|^2}{\hbar^2}\left\{\theta(t) + \theta(t-\tau) + \exp(-i\Phi)\exp\left[-\left(i\Delta_{21} + \frac{1}{T_{21}}\right)T\right]\theta(t-\tau) + \exp(i\Phi)\exp\left[\left(i\Delta_{21} - \frac{1}{T_{21}}\right)T\right]\theta(t-\tau)\right\}, \quad (6)$$

where $\Delta_{21} = \omega_{21} - \Omega_L$ is the detuning of the laser from the exciton transition. We can see that the last two terms express the interference between the coherence left in the medium by the first pulse with the excitation created by the second pulse. Thus, if $T_{21} \rightarrow \infty$, then for $\Phi = 0$ all the terms will add up coherently, leading to a fourfold increase in the population ρ_{22}. Because the THz radiation is proportional to the second derivative of the population, only the population **changes** matter. Differentiation up to the second order of Eq. (6) gives a nonanalytical result, but Eq. (6) still illustrates that, when there is coherent addition ($\Phi = 0$), the THz transient caused by the second pulse should be stronger and that, when the excited level is depopulated ($\Phi = \pi$), the THz transient should be opposite in sign compared with the THz waveform generated by the first pulse. When we numerically solve the optical Bloch equations and include a finite dephasing time and detuning, the calculation resembles the measurements shown in Fig. 19. The absence of these effects when continuum e–h pairs are excited becomes clear: dephasing times of continuum e–h pairs are of the order of 100 fs, giving a rapid decay of the optical coherence stored in the medium by the first pulse.[28] There is therefore no coherent interaction with the second pulse, and both pulses will excite practically identical numbers of polarized e–h pairs. In addition, the 2D-continuum states are inhomogeneously broadened,[29] which leads to a rapid decay of the phase coherence.

The depopulation of an exciton level by an incoming optical field means that a photon is emitted when the optical field excites the exciton system. This is basically a process of stimulated emission. It has long been known that a 180° shift in the exciting field driving an oscillating dipole can induce stimulated emission instead of absorption. The stimulated emission caused by the second optical pulse in our experiments requires the presence of a macroscopic coherence, though. This requirement is quite different from the usual treatment of stimulated emission in lasing media: although by definition the optical field causing the stimulated emission and the oscillating dipole are coherent, there is no requirement of a macroscopic coherence on the statistical ensemble of oscillating dipoles. Our experiments lie somewhere between these simple arguments of stimulated emission and recent developments in lasing without inversion,[30] where long dephasing times or coherence in the system is extremely important.

The process leading to THz radiation described in this section is closely related to previous research on virtual excitations and its implications for nonlinear phenomena.[31,32] When the detuning of the laser from the exciton transition is large enough, there are no real excitations left in the system after the laser pulse is gone. However, during the time when the laser excites the sample there is a virtual population of excitons that are being continuously excited and de-excited. These virtual population changes should also emit THz radiation, and from a nonlinear-optics point of view it is equivalent to difference-frequency mixing through a nonresonant nonlinearity. Some experimental evidence of THz emission caused by these virtual processes was found in Ref. 33 and is theoretically discussed in Ref. 34.

7. CONCLUSIONS AND SUMMARY

Coherent detection of far-infrared radiation has become a very powerful tool in the study of coherent phenomena in semiconductors. It is a unique tool in the sense that we can monitor the time evolution of the amplitude and the phase of $\chi^{(2)}$ processes in multilevel systems. From

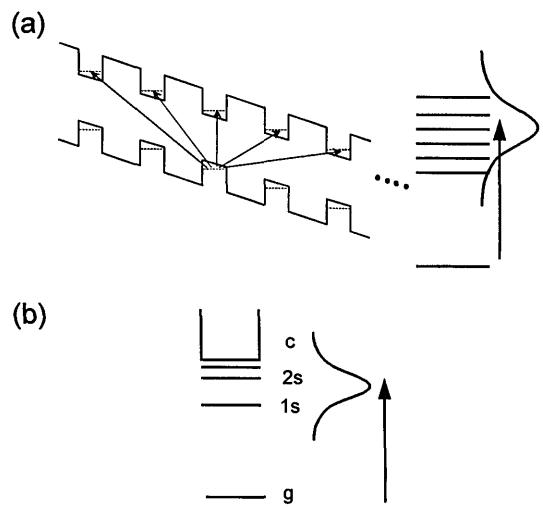

Fig. 22. Schematic diagram of other multilevel systems in semiconductor heterostructures studied in Refs. 6 and 37 that can be used for population and coherence control through adequate shaping of the exciting optical field.

these observations we can infer the time evolution of wave packets in these systems. Wave-packet dynamics has recently become a research field in its own right, and it draws concepts from time-dependent quantum mechanics and semiclassical models. For example, there are very active research efforts in wave-packet dynamics in Rydberg atoms.[35,36] Despite the dissimilarity of Rydberg atoms and excitons in semiconductor heterostructures, they share the same concepts when we confine ourselves to the study of wave-packet dynamics. The work described in this paper deals with quasi-three- and quasi-two-level systems implemented by excitonic levels in properly designed semiconductor heterostructures. Limiting the number of levels to three has the advantage of simplifying the physical phenomena and its modeling while still permitting the study of the basic physics of coherent processes. The extrapolation to more levels is not difficult, though. Recent experiments by Feldmann *et al.*[37] and Waschke *et al.*[6] have gone one step further in that they involved the study of wave-packet dynamics in semiconductor heterostructures with more than three levels. In the former study the multilevel system is provided by the ground and the excited states of the hh exciton in a SQW. The work conducted by the latter group focused on Bloch oscillations in a semiconductor superlattice under the application of an electric field. In the study of Waschke *et al.*[6] the multilevel system consists of the Wannier–Stark ladder that appears after the application of the electric field.[38] These two systems are depicted in Fig. 22. Although these groups used a single short laser pulse as the excitation field, it is not difficult to foresee coherent-control experiments with optical fields shaped in ways similar to the shaping we have used. An interesting concept for future experiments is the testing of population and coherence control through arbitrarily shaped pulses[39] in semiconductor heterostructures.

In summary, we have shown that it is possible to control the THz radiation from charge oscillations and the exciton populations in quantum wells by proper shaping of the exciting optical pulse. We have used two techniques for shaping the amplitude and the phase of the optical field: phase-locked pulse generation in a Michelson interferometer and pulse-train generation by phase-only filtering. We have discussed two main mechanisms for the generation of THz radiation from semiconductor quantum wells: charge oscillations and THz radiation from population changes. We have shown that by proper manipulation of the exciting field we can enhance, weaken, or phase shift the THz field produced by charge oscillations. Also, we have demonstrated that, when a pulse train with an adequate repetition rate excites the sample, forced charge oscillations exist. Finally, we have taken advantage of the longer dephasing time of excitons compared with free carriers for active control of their populations and hence of the THz radiation that follows the creation or the destruction of polarized e–h pairs.

ACKNOWLEDGMENTS

We thank K. Köhler for providing the DCQW sample, G. E. Doran and B. Tell for technical assistance, and W. H. Knox and D. A. B. Miller for valuable discussions.

*Present address, AT&T Bell Laboratories, 600 Mountain Avenue, Murray Hill, New Jersey 07974.

†Present address, University of Technology Delft, Technische Natuurkunde, Lorentzweg 1, 1628 CJ Delft, The Netherlands.

REFERENCES AND NOTES

1. D. S. Kim, J. Shah, D. A. B. Miller, W. Schäefer, and L. Pfeiffer, Phys. Rev. B **48,** 17902 (1993).
2. J.-Y. Bigot, M.-A. Mycek, S. Weiss, R. G. Ulbrich, and D. S. Chemla, Phys. Rev. Lett. **70,** 3307 (1993).
3. H. G. Roskos, M. C. Nuss, J. Shah, K. Leo, D. A. B. Miler, A. M. Fox, S. Schmitt-Rink, and K. Köhler, Phys. Rev. Lett. **68,** 2216 (1992).
4. P. C. M. Planken, M. C. Nuss, W. H. Knox, D. A. B. Miller, and K. W. Goossen, Appl. Phys. Lett. **61,** 2009 (1992).
5. P. C. M. Planken, M. C. Nuss, I. Brener, K. Goosen, M. S. C. Luo, S.-L. Chuang, and L. Pfeiffer, Phys. Rev. Lett. **69,** 3800 (1992).
6. C. Waschke, H. G. Roskos, R. Schwedler, K. Leo, H. Kurz, and K. Köhler, Phys. Rev. Lett. **70,** 3319 (1993).
7. J. T. Fourkas, W. L. Wilson, G. Wäckerle, A. E. Frost, and M. D. Fayer, J. Opt. Soc. Am. B **6,** 1905 (1989).
8. W. S. Warren and A. H. Zewail, J. Chem. Phys. **78,** 2279 (1983).
9. M. M. Solour and C. Cohen-Tannoudji, Phys. Rev. Lett. **38,** 757 (1977).
10. N. F. Scherer, R. J. Carlson, A. Matro, M. Du, A. J. Ruggiero, V. Romero-Rochin, J. A. Cina, G. R. Fleming, and S. A. Rice, J. Chem. Phys. **95,** 1487 (1991).
11. A. Villaeys and K. F. Freed, Chem. Phys. **13,** 271 (1976).
12. J.-C. Diels and J. Stone, Phys. Rev. A **31,** 2397 (1985).
13. A. M. Weiner, D. E. Leaird, G. P. Wiederrecht, and K. A. Nelson, Science **247,** 1317 (1990).
14. M. S. C. Luo, S. L. Chuang, P. C. M. Planken, I. Brener, H. G. Roskos, and M. C. Nuss, IEEE J. Quantum Electron. **30,** 1478 (1994).
15. M. C. Nuss, P. C. M. Planken, I. Brener, H. G. Roskos, M. S. C. Luo, and S. L. Chuang, Appl. Phys. B **58,** 249 (1994).
16. P. R. Smith, D. H. Auston, and M. C. Nuss, IEEE J. Quantum Electron. **24,** 255 (1988).
17. A. M. Weiner and D. E. Leaird, Opt. Lett. **15,** 51 (1990).
18. A. M. Weiner, J. P. Heritage, and E. M. Kirschner, J. Opt. Soc. Am. B **5,** 1563 (1988).
19. P. C. M. Planken, I. Brener, M. C. Nuss, M. S. C. Luo, and S. L. Chuang, Phys. Rev. B **48,** 4903 (1993).
20. M. S. C. Luo, S. L. Chuang, P. C. M. Planken, I. Brener, and M. C. Nuss, Phys. Rev. B **48,** 11043 (1993).
21. Obviously these three dephasing times are related to one another, and T_{23}, $T_{13} \geq T_{12}$. Calculations assuming different parameters show that the physical picture is unchanged. The use of these parameters does not imply the assumption of homogeneous broadening for all the transitions; these parameters should be regarded more as effective dephasing times. Despite the fact that our exciton transitions are most probably inhomogeneously broadened, we did observe a Lorentzian line shape in the THz emission by charge oscillations, which indicates homogeneous broadening for the $1 \rightarrow 2$ transition.
22. Y. R. Shen, *The Principles of Nonlinear Optics*, 1st ed. (Wiley, New York, 1984), Chap. 2, p. 13.
23. W. S. Warren, H. Rabitz, and M. Dahleh, Science **259,** 1581 (1993).
24. I. Brener, P. C. M. Planken, M. C. Nuss, L. Pfeiffer, D. E. Leaird, and A. M. Weiner, Appl. Phys. Lett. **63,** 2213 (1993).
25. S. L. Chuang, S. Schmitt-Rink, B. I. Greene, P. N. Saeta, and A. F. J. Levi, Phys. Rev. Lett. **68,** 102 (1991).
26. Some fine structure is still observed in the case of the SQW because the quantum-beat frequency shifts with the application of an electric field (unlike the case of the DCQW sample).
27. P. C. M. Planken, I. Brener, M. C. Nuss, M. S. C. Luo, S. L. Chuang, and L. N. Pfeiffer, Phys. Rev. B **49,** 4668 (1994).

28. D. S. Kim, J. Shah, J. E. Cunningham, T. C. Damen, W. Schäfer, M. Hartmann, and S. Schmitt-Rink, Phys. Rev. Lett. **68,** 1006 (1992).
29. P. C. Becker, H. L. Fragnito, C. H. Brito Cruz, R. L .Fork, J. E. Cunningham, J. E. Henry, and C. V. Shank, Phys. Rev. Lett. **61,** 1647 (1988).
30. For a review, see M. O. Scully and M. Fleischhauer, Science **263,** 337 (1994).
31. M. Yamanishi, Phys. Rev. Lett. **59,** 1014 (1987).
32. D. S. Chemla, D. A. B. Miller, and S. Schmitt-Rink, Phys. Rev. Lett. **59,** 1018 (1987).
33. B. B. Hu, X.-C. Zhang, and D. H. Auston, Phys. Rev. Lett. **67,** 2709 (1991).
34. A. V. Kuznetsov and C. J. Stanton, Phys. Rev. B **48,** 10,828 (1993).
35. A. ten Wolde, L. D. Noordam, A. Lagendijk, and H. B. van Linden van den Heuvell, Phys. Rev. Lett. **81,** 2090 (1988).
36. J. A. Yeazell and C. R. Stroud, Phys. Rev. Lett. **60,** 1494 (1988).
37. J. Feldmann, T. Meier, G. von Plessen, M. Koch, E. O. Göbel, P. Thomas, G. Bacher, C. Hartmann, H. Schweizer, W. Schäfer, and H. Nickel, Phys. Rev. Lett. **70,** 3027 (1993).
38. See, for example, C. Weisbuch and B. Vinter, *Quantum Semiconductor Heterostructures, Fundamentals, and Applications* (Academic, London, 1991), p. 92.
39. S. Shi, A. Woody, and H. Rabitz, J. Chem. Phys. **88,** 6870 (1988).